ACS OMEGA

Open Access

http://pubs.acs.org/journal/acsodf

Article

Aluminum Dust Explosion Suppression Performance and Mechanism of a New Mesoporous Composite Explosion Suppressant

Xinyu Li, Haiyan Chen,* Yansong Zhang, Chunmiao Yuan, Hongzhao Wei, Wenxue Sun, Zhangjie Lu, and Qingzhou Zhang

Cite This: *ACS Omega* 2024, 9, 44942−44955

Read Online

ACCESS | Metrics & More | Article Recommendations

ABSTRACT: In this paper, using a 20 L spherical explosive device and a Hartmann device, we carried out explosion suppression experiments on 19 and 30 μm aluminum powders (500 g/m^3) with different concentrations of the new explosive suppressants (MCM41@CS-APP) and $CaCO_3$ and elaborated on the suppression mechanism of the explosion of MCM41@CS-APP on aluminum powder. The experimental results show that when the concentration of the explosion suppressor is 50 g/m^3, the maximum explosion pressure (P_{max}) produced by the explosion of mixed dust is higher than that of the explosion of aluminum powder, and with the increase of the concentration of the deflagration suppressant, the P_{max} of the mixed dust decreases. When the concentrations of MCM41@CS-APP and $CaCO_3$ reached 400 g/m^3, the P_{max} of the mixed dust (Al = 19 μm) was 0.133 and 0.364 MPa, which decreased by 81.3% and 48.9%, respectively. The P_{max} of the mixed dust (Al = 30 μm) was not significant. Both detonation inhibitors inhibited the explosion of aluminum powder; the detonation duration of Al/MCM41@CS-APP is shorter; there are fewer aluminum particles in the product; and the initial oxidation temperature of aluminum powder is higher.

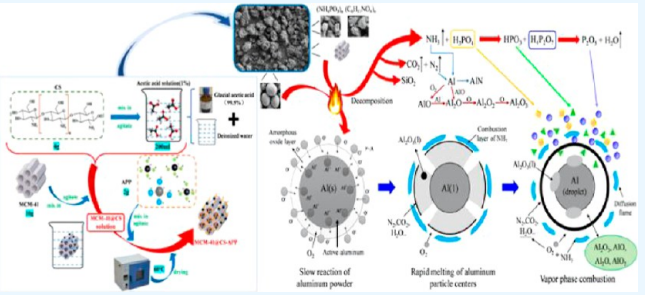

1. INTRODUCTION

Aluminum (Al) is an important raw metal material widely used in the metal manufacturing and metallurgy fields. Since the 21st century, the rapid development of the finishing industry, especially in the polishing and grinding processes of Al products, has generated large amounts of Al dust. As the Al dust accumulates to a certain concentration in a limited space and encounters an ignition source, it may explode or cause severe consequences. Therefore, Al dust explosion prevention is of great significance, and the explosion suppression characteristics and mechanism are the basis for Al dust explosion suppression. Al dust explosion suppression has been extensively studied, and great progress has been made.[1−3]

Due to the extremely high activity of Al, different materials including inert gas, fine water mist, and solid powder antiexplosion agents (phosphate, carbonate, etc.) have been studied in depth for their explosion suppression effects, and their suppression characteristics and laws are explored.[4−7] To evaluate the dust explosion suppression abilities of $NaHCO_3$ and $NH4H_2PO_4$, Amrogowicz et al., respectively, injected the suppressants into a container and measured the sum of the explosion lower limits.[8] They found that the explosion suppression effect of $NH_4H_2PO_4$ was better than that of $NaHCO_3$. Jiang et al. revealed by observing the flame shape of Al dust deflagration that the maximum flame speed decreased with the increase of the inhibitor concentration, and the inhibition effect of $NH_4H_2PO_4$ was better than that of $NaHCO_3$.[9] Zhang and Bi et al. studied the suppression effects of CO_2 and H_2 on the explosion of Al dust in a closed cuboid space and found that their suppression mechanisms were different, and the suppression effect of CO_2 was significantly better than that of H_2.[10] Zhang et al. developed the ATH/ZB composite explosion inhibitor by physical/chemical synthesis.[11] The minimum inhibitory concentrations of ATH and ZB alone for the aluminum dust explosion were 1000 g/m^3, while that of ATH/ZB was only 600 g/m^3. They also studied the suppression mechanism of NZB on the Al dust explosion and demonstrated that the suppression performance of NZB was better than that of ZB2335.[12] Dai et al. compared the Al dust explosion suppression abilities of NaH_2PO_4, $(NH_4)_2HPO_4$, $NH_4H_2PO_4$, $KHCO_3$, and $NaHCO_3$ using a 20 L spherical explosion device and found that 40% NaH_2PO_4 could completely suppress the explosion of Al dust, while 50% $(NH_4)_2HPO$ and 50% $NH_4H_2PO_4$ showed obvious

Received: April 23, 2024
Revised: August 27, 2024
Accepted: September 9, 2024
Published: October 28, 2024

suppression effects.[13] Ke and Meng et al. obtained the KH_2PO_4/SiO_2 composite deflagration suppressant by mixing and grinding the two raw materials and explored its suppression effect in a Hartmann tube.[14] The results revealed that the flame propagation of Al powder deflagration could be effectively suppressed with 60% KH_2PO_4/SiO_2 and completely suppressed with 90% KH_2PO_4/SiO_2. Deng et al. measured the explosion degrees of Al/ABC, Al/MCA, and Al/ABC/MCA mixtures, respectively, using a vertical explosion tube device and analyzed the explosion suppression effects of different suppressant powders.[15] The results showed that the suppression effect of ABC was the worst, followed by ABC/MCA, and that of MCA was the best.

Composite powder explosion suppressants exhibit synergistic effects, leading to superior explosion suppression performance compared to that of single powder suppressants. At present, the study of the development of composite solid explosion suppressants and the study of their suppression performances are urgently needed. Due to its large specific surface area, good thermal stability, and high porosity,[16,17] mesoporous SiO_2 has been rapidly developed in the fields of catalysis, adsorption, and biomedicine.[18−20] Ammonium polyphosphate (APP) and chitosan (CS) are good flame retardants,[21−24] where APP serves as the acid and gas source of the flame retardant system, and CS serves as the carbon source. Herein, a new mesoporous composite explosion powder suppressant, MCM41@CS-APP, was prepared by functionally modifying the surface of mesoporous SiO_2.[25] Since $CaCO_3$ has a good inhibitory effect on dust explosion,[26−28] the article used MCM41@CS-APP and $CaCO_3$ to carry out the explosion inhibition experiment of aluminum powder to obtain the effect of the two on the explosion pressure and combustion flame of aluminum powder. Based on the scanning electron microscopy (SEM), thermogravimetric analysis (TGA), and X-ray photoelectron spectroscopy (XPS) analyses of the explosion products, the inhibition performance and inhibition mechanism of MCM41@CS-APP on the explosion of aluminum powder were obtained, which not only improved the study on the Al dust explosion suppression by the composite solid explosion suppressant but also provided theoretical support for the development of effective prevention and control techniques and equipment for Al dust explosion accidents.

2. EXPERIMENTS

2.1. Materials. *2.1.1. Al Powder.* The Al dust explosion accident occurred in Jiangsu Kunshan Zhongrong Metal Products Co., Ltd. in 2014 was taken as the research background. Based on the site conditions, spherical Al powders with particle sizes of 19 and 30 μm (Henan Yuanyang Powder Technology Co., Ltd.) were selected as the research subjects. The physical properties of the Al powders are shown in Table 1.

The particle size distributions of the 19 and 30 μm Al powders were measured with a laser diffractometer. As shown in Figure 1, the particle sizes of the 19 μm Al powder mainly fell in the range of 15.1−22.9 μm, and its Sauter mean diameter $D^{2,3}$ and De Brouckere mean diameter $D^{3,4}$ were measured to be 19.3 and 21.3 μm, respectively.

Table 1. Physical Properties of 19 μm/30 μm Al Powders

		elemental composition				
	appearance	Al (%)	Fe (%)	Cu (%)	Si (%)	H_2O (%)
19 μm	silver gray, no aggregations	99.78	0.1018	0.0012	0.0422	0.02
30 μm	silver gray, no aggregations	99.64	0.1037	0.0019	0.0527	0.03

2.1.2. $CaCO_3$. $CaCO_3$ was purchased from Shanghai Macklin Biochemical Co., Ltd. (Shanghai, China). Its physical properties are listed in Table 2. Figure 2 shows the scanning electron microscopy image of $CaCO_3$.

2.1.3. MCM41@CS-APP. The MCM-41 molecular sieve was provided by Nankai University Catalyst Co., Ltd. (Nanjing, China). Its physical properties are listed in Table 3.

To synthesize MCM41@CS-APP, 4 g of CS was added into 200 mL of 1% acetic acid solution (2 mL of glacial acetic acid + 200 mL of deionized water) and stirred until completely dissolved. Ten g of MCM-41 molecular sieve was added into the CS solution, and the mixture was vigorously stirred for 1 h. The pH of the suspension was adjusted to 13 with 0.05 mol/L NaOH. Two g of APP powder was added into the suspension and stirred thoroughly. The suspension was centrifuged, and the residue was washed with deionized water until it became neutral and dried under vacuum at 60 °C to obtain MCM41@CS-APP.[29]

Figure 3 shows the schematic diagram for the synthesis of MCM41@CS-APP, and its microscopic morphology is presented in Figure 4.

2.2. Experimental Equipment. To explore the Al dust explosion suppression mechanism of the mesoporous composite explosion suppressant, the pressures and flame evolutions during the deflagration of Al powder and mixed dust were tested using a 20 L spherical explosion apparatus and a dust cloud energy measurement system as recommended by international standard ISO 6184-1[30] and the national standard GB/T 16425.[31]

2.2.1. 20 L Spherical Explosion Apparatus. The 20 L spherical explosion apparatus used for the explosion experiments was mainly composed of an explosion chamber, a powder diffuser, a pneumatic control system, an ignition device, and a data acquisition and control system. Figure 5 shows a schematic diagram of the apparatus structure. The chemical igniters of zirconium, barium nitrate, and barium peroxide have a weight ratio of 4:3:3, and the energy release of 0.48 g chemical igniter corresponds to 2 kJ. After mixing the experimental dust evenly, it was spread evenly into the powder storage chamber. The explosion chamber was evacuated to 0.06 MPa, and the dust storage chamber was pressurized to 2 MPa. Once the operation parameters were set by the computer control software and gas distribution was calculated and set by the gas distribution system, the start valve was open. The explosion pressure evolutions were measured by a pressure sensor installed in the vessel wall and recorded by a data acquisition system for each run. These data yielded values of the maximum explosion pressure (P_{max}) and maximum rate of pressure rise (dP/dt_{max}).

2.2.2. Dust Cloud Energy Measurement System. The dust cloud energy measurement system was mainly composed of a Hartmann tube, an electric spark energy generator, an air compressor, and a solenoid valve. Figure 6 shows the schematic diagram of the system. The dust was placed under the Hartmann tube and adjusted to the position of the two electrodes to make them vertical and facing each other. The pressure was raised to 0.5 MPa with the air pump. The solenoid valve was turned on to blow the dust into the cylindrical glass tube. The spark energy generator was turned on to output an ignition energy of 20 J. The flame evolution of the dust cloud during the combustion process was recorded with a high-speed camera.

https://doi.org/10.1021/acsomega.4c03871
ACS Omega 2024, 9, 44942−44955

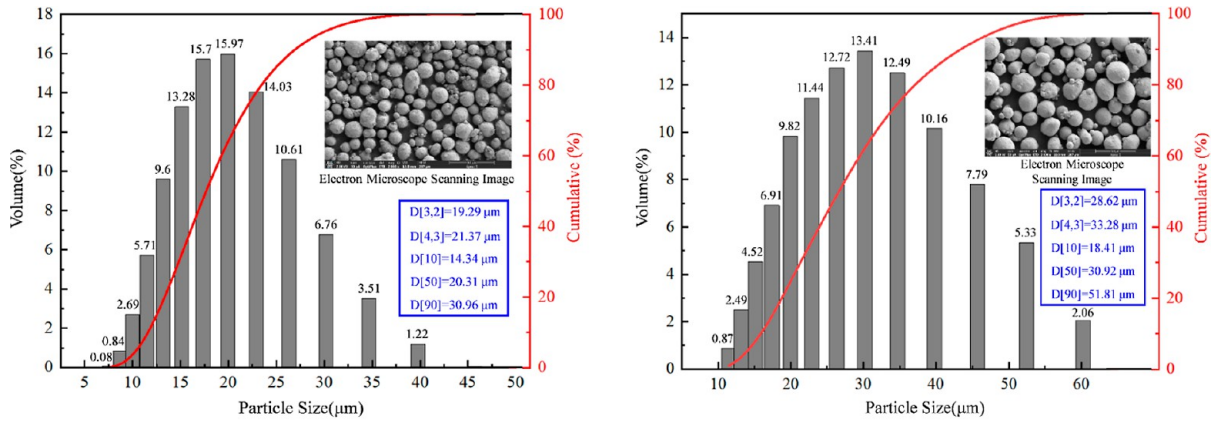

(a) 19 μm Al powders (b) 30 μm Al powders

Figure 1. Particle size distributions and SEM images of Al powders.

Table 2. Physical Properties of $CaCO_3$

appearance	melting point	decomposition temperature	density	water solubility
white powder	1339 °C	825−896 °C	2.93 g/cm^3 (25 °C)	insoluble

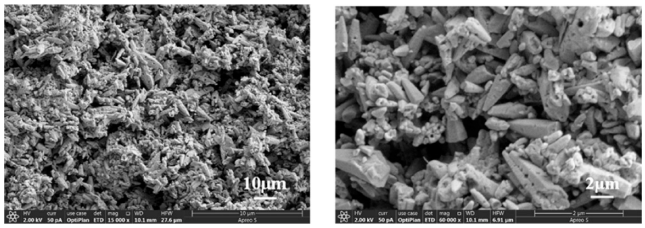

Figure 2. SEM images of $CaCO_3$.

Table 3. Physical Properties of MCM-41

proportion of silicon	relative crystallinity	pore diameter	specific surface area
100%	≥95%	3.8 nm	1180 m^2/g

3. EXPLOSION EXPERIMENTS OF AL POWDER AND MIXED DUSTS

3.1. Explosion Overpressure of Al Powder. In order to determine the optimal explosion concentration of aluminum powder, explosion experiments were conducted on the 19 and 30 μm Al powders at concentrations in the ranges of 50−750 and 50−850 g/m^3, respectively, and the aluminum powder at each concentration was subjected to three explosion tests. Their maximum explosion pressures (P_{max}) and the maximum rates of explosion pressure rise (dP/dt_{max}) are shown in Figure 7.

The P_{max} of 19 and 30 μm Al powders both increase first and then decrease with the increase of concentration (Figure 7a). The highest P_{max} = 0.796 MPa of 19 μm Al powder is obtained at a concentration of 650 g/m^3, while the P_{max} of 30 μm Al powder reaches the maximum of 0.646 MPa at a concentration of 500 g/m^3. Their dP/dt_{max} values also show the same increasing and decreasing trends with the increase of concentration (Figure 7b). The highest dP/dt_{max} of the 19 μm Al powder is 27.07 MPa/s, and that of the 30 μm Al powder is 12.89 MPa/s. Smaller particle sizes are conducive to oxygen diffusion,[32] and their larger surface areas provide larger contact areas with oxygen. Therefore, at the same concentration, the Al powder with the smaller particle sizes causes more violent explosions.[33,34]

Based on the analyses above and the capacity of the experimental equipment, the Al powder concentration was set to 500 g/m^3 in the subsequent experiments.

3.2. Effects of the Explosion Suppressant on Explosion Overpressure. With the concentration of Al powder at 500 g/m^3, the concentration of $CaCO_3$ in the mixed dust was varied to 50, 100, 200, 300, 400, and 500 g/m^3, and that of MCM41@CS-APP was varied to 50, 100, 200, 300, and 400 g/m^3, respectively. The maximum explosion pressures generated by these mixed dusts are listed in Figure 8.

As shown in Figure 8, at the fixed aluminum powder concentration, P_{max} shows downward trends with the increases of the concentrations of MCM41@CS-APP and $CaCO_3$. At the same suppressant concentration, the P_{max} produced by the reaction of the Al powder (19 μm)/suppressant is higher than that of the Al powder (30 μm)/suppressant (except for at the suppressant concentration of 50 g/m^3), suggesting that the explosive power of Al powder with a smaller particle size is greater. As 50 g/m^3 of MCM41@CS-APP was added, the P_{max} of the Al powders increased to 0.725 and 0.669 MPa, respectively, higher than those generated by the pure Al powders. The same phenomenon is observed as 50 g/m^3 of $CaCO_3$ is added. These observations indicate that low concentrations of the suppressant can promote the explosion of Al dust. Amyotte et al. analyzed this phenomenon and believed that the decomposition of the low concentration of the suppressant in the high-temperature environment could enhance the explosion.[35,36] Both MCM41@CS-APP and $CaCO_3$ significantly inhibited the explosion of aluminum powder when the concentration of the suppressant reached 400 g/m^3. The P_{max} of the mixed dust (Al = 19 μm) was 0.133 and 0.364 MPa, which decreased by 81.3% and 48.9%, respectively. The P_{max} of the mixed dust (Al = 30 μm) was not significant.

In addition, the aluminum powder particle size is unchanged; adding the same concentration of detonation inhibitor, Al/MCM@CS-APP-produced P_{max} is lower than that produced by Al/$CaCO_3$, preliminary indication that the detonation inhibition effect of MCM41@CS-APP is significantly better than that of $CaCO_3$.

https://doi.org/10.1021/acsomega.4c03871
ACS Omega 2024, 9, 44942−44955

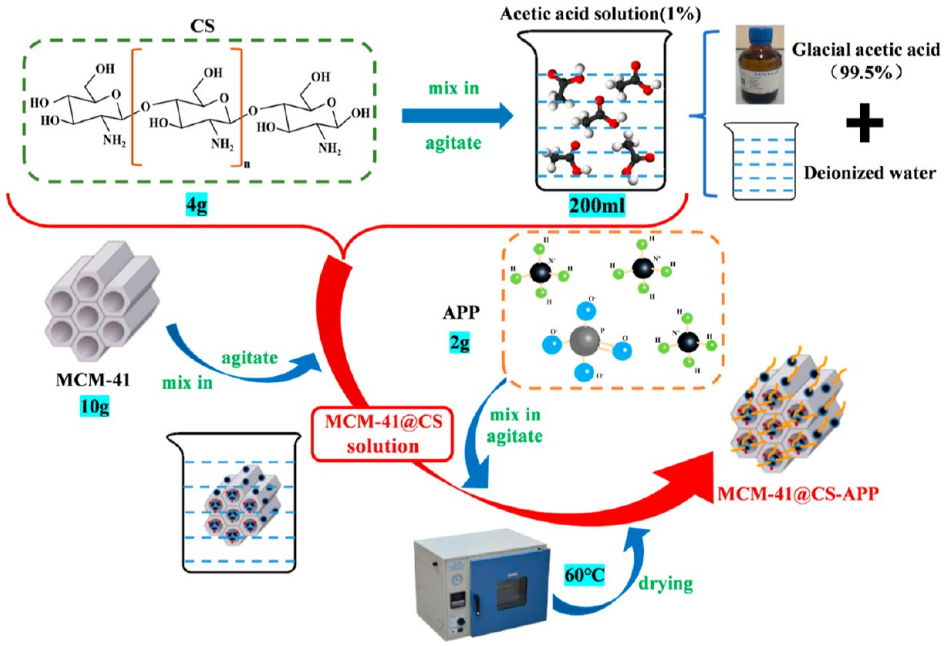

Figure 3. Schematic diagram of the synthesis of MCM41@CS-APP.

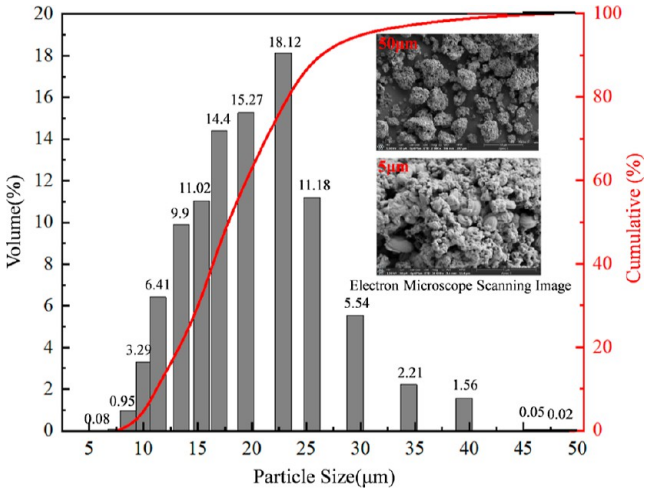

Figure 4. Particle size distributions and SEM images of MCM41@CS-APP.

4. EXPERIMENTAL STUDY ON FLAME EVOLUTION DURING DEFLAGRATION

4.1. Flame Evolution during Al Powder Deflagration.

Figure 9 shows the flame evolution during the deflagration of 19 and 30 μm aluminum powders (500 g/m^3) recorded by the dust cloud ignition energy measurement system.

As shown in Figure 9a, under a pressure of 0.5 MPa, the Al powder quickly fills into the Hartmann tube. At 379 ms, the Al dust is ignited, and then the flame spreads upward along the Hartmann tube. At 530 ms, the flame rushes out of the tube and develops most violently. During the period of 530−602 ms, the flame near the tube mouth gradually disappears because of the reaction of Al dust in the upper part of the tube ends. Meanwhile, the relative high concentration of Al powder in the middle and lower parts of the tube maintains the flame at the bottom, and the disappearance of the flame is relatively slow. At 707 ms, the deflagration of the Al powder is over, and the flame is no longer observed. The deflagration of the 19 μm Al powder lasts 328 ms.

As observed from Figure 9a, 30 μm aluminum powder combustion lasted for 314 ms, and the initial combustion moment of 30 μm aluminum powder is 27 ms later, which indicates that the aluminum powder with a smaller particle size is easier to ignite.

4.2. Flame Evolution during Mixed Dust Deflagration.

4.2.1. Flame Evolution during Mixed Dust Deflagration (Al = 19 μm). Based on the deflagration flame evolution of 19 μm Al powder, 200 and 400 g/m^3 of MCM41@CS-APP and $CaCO_3$ were, respectively, mixed with the Al powder. The deflagration flame evolution laws of the four mixed dusts are obtained, as shown in Figures 10 and 11.

In Figure 10a, the fire of mixed dust Al/MCM41@CS-APP appeared at 389 ms, which was 10 ms later than the initial reaction time of Al/MCM41@CS-APP compared to Figure 9a; the reaction degree of Al/MCM41@CS-APP reached the maximum at 477 ms; and the combustion of the mixed dust was near the end at 671 ms. Its reaction process is 282 ms, which is 46 ms shorter than the reaction maintenance time of aluminum powder. As shown in Figure 10b, Al/$CaCO_3$ starts to react at 398 ms, which is later than the initial reaction time of aluminum powder, and its reaction process duration is 305 ms, which is 23 ms shorter than the reaction maintenance time of aluminum powder.

In Figure 11, the degree of flame development of the two mixtures of dusts was significantly reduced after addition of 400 g/m^3 of the deflagration suppressant to the aluminum powder. In Figure 11a, the initial reaction moment of Al/MCM41@CS-APP was unchanged, but the flame development to the optimum extent was delayed by 99 ms compared with that in Figure 10a, and the flame extinguished more quickly.

4.2.2. Flame Evolution during Mixed Dust Deflagration (Al = 30 μm). Based on the deflagration flame evolution of 30 μm Al powder, 200 and 400 g/m^3 of MCM41@CS-APP and $CaCO_3$ were, respectively, mixed with the Al powder. The deflagration flame evolution laws of the four mixed dusts are obtained, as shown in Figures 12 and 13.

https://doi.org/10.1021/acsomega.4c03871
ACS Omega 2024, 9, 44942−44955

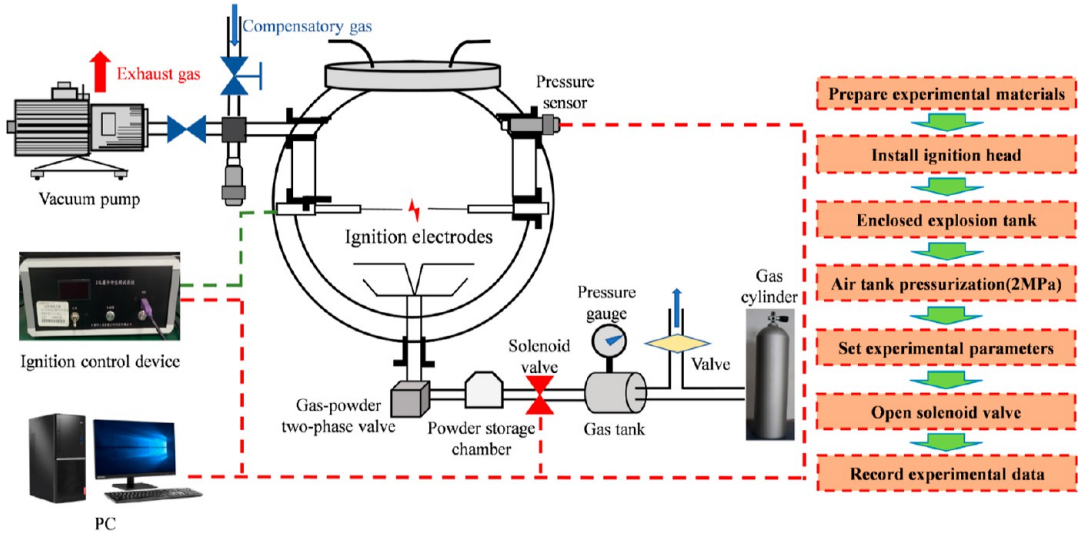

Figure 5. Schematic diagram of 20 L spherical explosion apparatus.

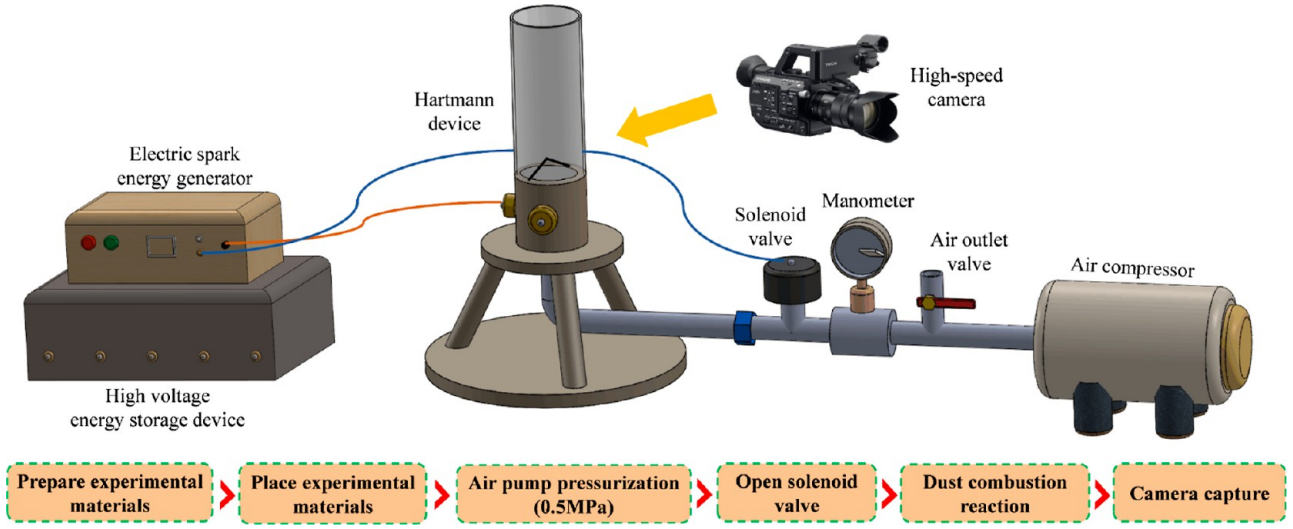

Figure 6. Schematic diagram of the dust cloud energy measurement system.

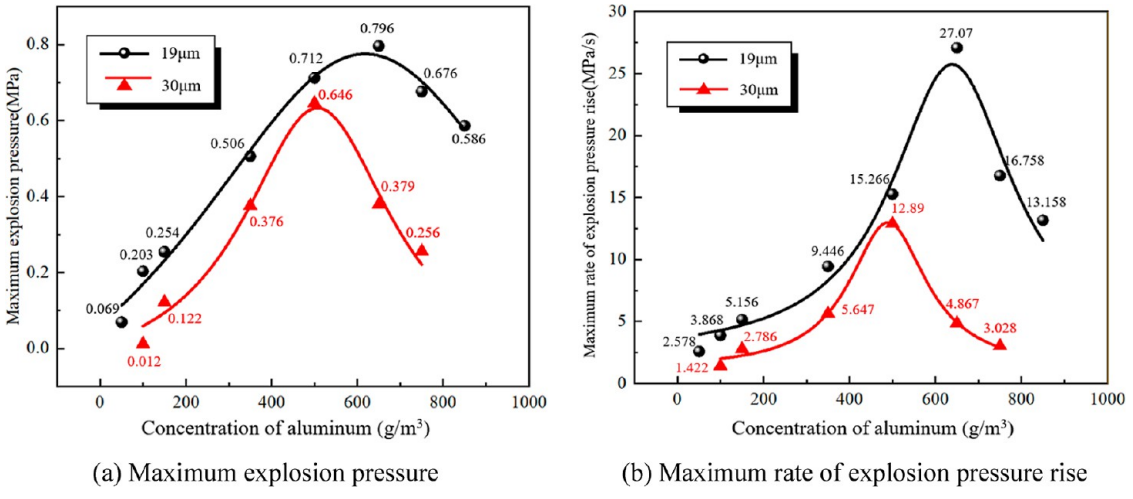

Figure 7. Maximum explosion pressures and maximum rates of explosion pressure rise of the two Al powders at different concentrations.

As shown in Figure 12a, the Al/MCM41@CS-APP reaction process is 266 ms, which is 48 ms shorter than the reaction sustaining time of aluminum powder (30 μm). As Figure 12b shows, the Al/$CaCO_3$ reaction process is 287 ms, and the

https://doi.org/10.1021/acsomega.4c03871
ACS Omega 2024, 9, 44942−44955

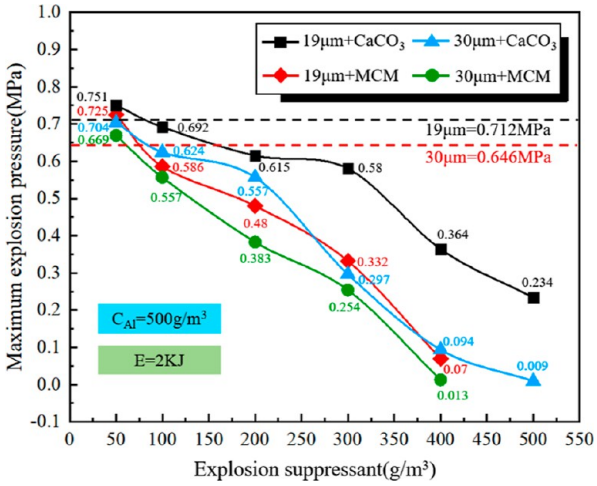

Figure 8. Maximum explosion pressures of Al/MCM41@CS-APP and Al/$CaCO_3$ mixed dusts containing different concentrations of the suppressant.

reaction sustaining time also appears to be scaled down. In Figure 13, the flame development of the mixed dust was substantially weakened by adding 400 g/m^3 of the deflagration suppressant to the aluminum powder. As displayed in Figure 13a, Al/MCM41@CS-APP reacted at 429 ms, and its reaction process reached 113 ms. In Figure 13b, the degree of reaction of Al/$CaCO_3$ was also significantly weakened, a stronger flame appeared in the 419−452 ms, and its initial reaction moment and the end of the reaction moment were advanced.

According to the above experiments, it is observed that:

(1) The concentration of suppressor is constant, and the larger the particle size of the aluminum powder, the shorter the reaction time of the mixed dust, and the weaker the flame development.

(2) Further verified that the inhibition of the burning of aluminum powder by MCM41@CS-APP is significantly better than that of $CaCO_3$, which is reflected in three aspects: the flame produced by Al/MCM41@CS-APP in the optimum degree is obviously weaker than that by Al/$CaCO_3$; adding the same concentration of MCM41@CS-APP and $CaCO_3$, the reaction time of Al/MCM41@CS-APP is much smaller than that of Al/$CaCO_3$, and the high-concentration MCM41@CS-APP shows significantly superior suppression effects in terms of flame brightness and flame height when compared to $CaCO_3$ (see Figure 14).

5. EXPLOSION RESIDUE ANALYSIS

5.1. Physical Form Analysis. *5.1.1. Microanalysis (SEM).* The explosion residues of 19 μm Al powder and Al powder/suppressant (50, 200, and 400 g/m^3) mixed dusts were characterized by SEM for their morphologies. The results are shown in Figures 15 and 16.

As can be seen from Figure 15, the particle size of Al_2O_3 produced from the explosion of Al powder is significantly smaller than the particle size of the Al powder. After 50 g/m^3 of MCM41@CS-APP was added to the 500 g/m^3 Al powder, different sizes of Al_2O_3 particles were observed in the explosion residue. As the MCM41@CS-APP concentration increased to 200 and 400 g/m^3, the number of Al particles drastically increased in the explosion residue, indicating that MCM41@

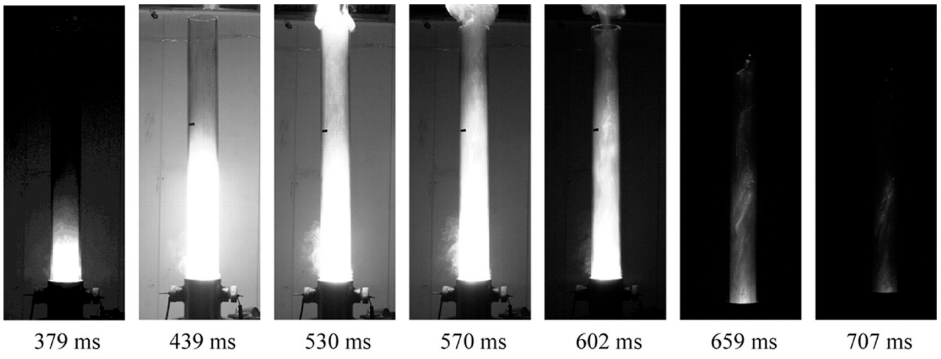

(a) Flame evolution during the deflagration of Al (19 μm)

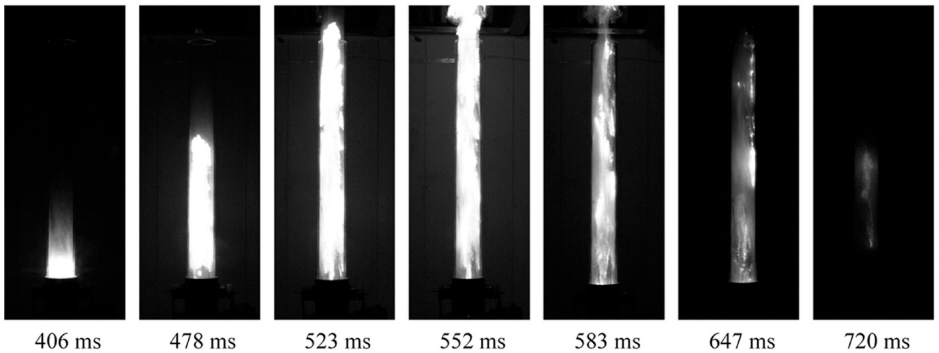

(b) Flame evolution during the deflagration of Al (30 μm)

Figure 9. Flame evolution during the deflagration of Al powder.

https://doi.org/10.1021/acsomega.4c03871
ACS Omega 2024, 9, 44942−44955

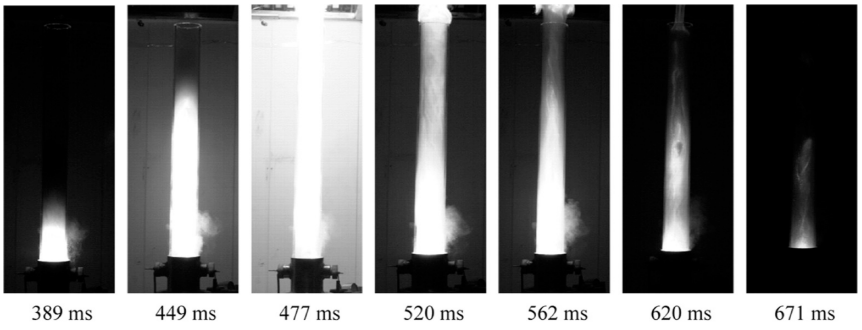

(a) Flame evolution during the deflagration of Al/MCM41@CS-APP

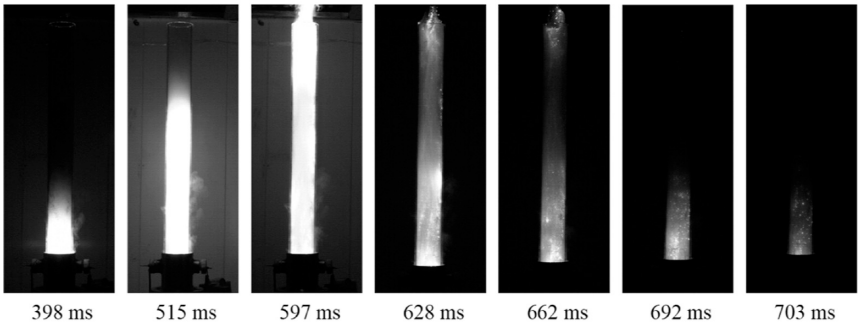

(b) Flame evolution during the deflagration of $Al/CaCO_3$

Figure 10. Flame evolutions during the deflagrations of Al/MCM41@CS-APP (200 g/m^3) and $Al/CaCO_3$ (200 g/m^3).

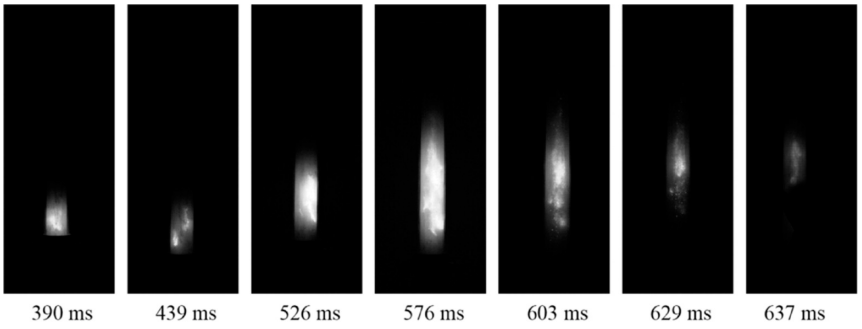

(a) Flame evolution during the deflagration of Al/MCM41@CS-APP

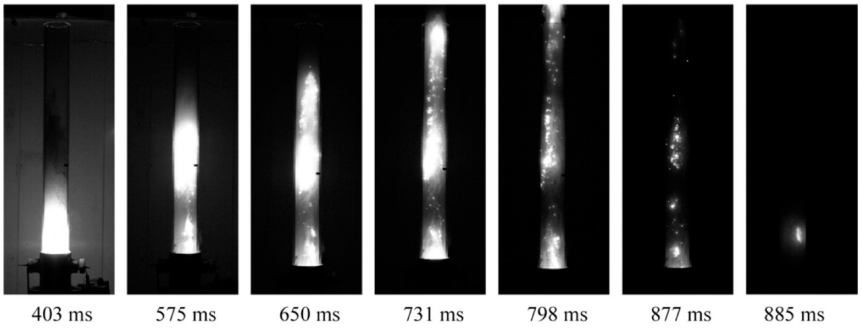

(b) Flame evolution during the deflagration of $Al/CaCO_3$

Figure 11. Flame evolutions during the deflagrations of Al/MCM41@CS-APP (400 g/m^3) and $Al/CaCO_3$ (400 g/m^3).

CS-APP can greatly inhibit the explosion of Al powder at those doses.

Similarly, after 50 and 200 g/m^3 $CaCO_3$ are respectively added to the Al powder, the SEM images reveal more Al_2O_3 particles and fewer Al particles in the explosion residues (Figure 16). As the $CaCO_3$ concentration increased to 400 g/m^3, more Al particles were found in the explosion residue, and the explosion suppression effect of $CaCO_3$ at this concentration is relatively obvious.

5.1.2. Macroanalysis. A uniform Al_2O_3 film is observed on the chamber wall after the Al powder explosion (Figure 17a). As 50 g/m^3 of MCM41@CS-APP is added, a layer of off-white substance is found at the lower part of the chamber, and there are flocculent reactants on the ignition electrode (Figure 17b). The

https://doi.org/10.1021/acsomega.4c03871
ACS Omega 2024, 9, 44942−44955

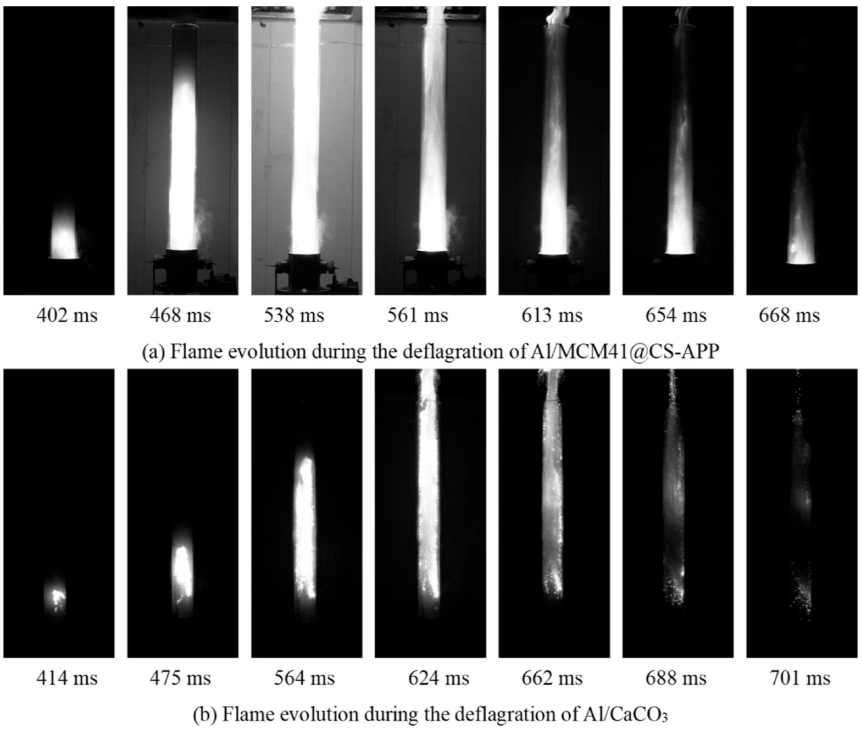

Figure 12. Flame evolutions during the deflagrations of Al/MCM41@CS-APP (200 g/m^3) and Al/$CaCO_3$ (200 g/m^3).

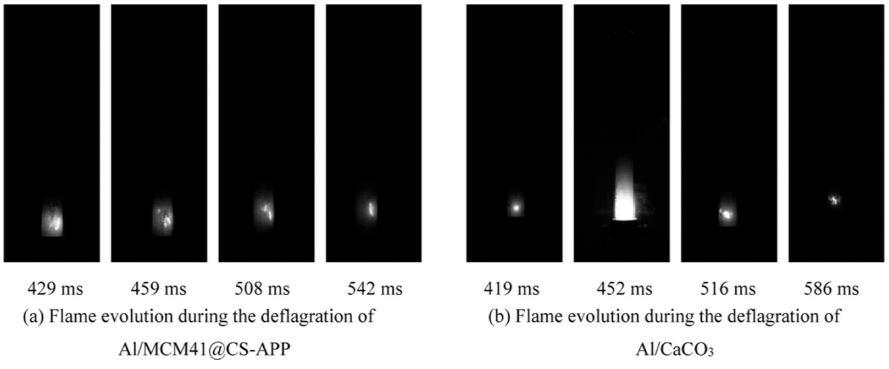

Figure 13. Flame evolutions during the deflagrations of Al/MCM41@CS-APP (400 g/m^3) and Al/$CaCO_3$ (400 g/m^3).

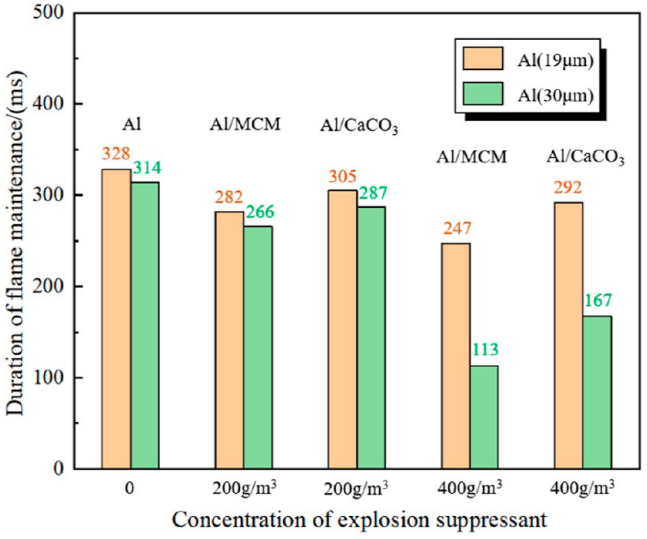

Figure 14. Durations of the deflagrations of different mixed dusts.

explosion residue of the mixed dust containing 200 g/m^3 MCM41@CS-AP at the bottom of the chamber is dark gray (Figure 17c), indicating that a dense layer of product of MCM41@CS-AP itself is formed at high temperature as more MCM41@CS-APP is added.[37] This dense layer prevents the reaction of a considerable amount of Al powder. At the MCM41@CS-APP concentration of 400 g/m^3, a dense white substance is formed on the surface of the aluminum powder due to the reaction of MCM41@CS-APP, which prevents the reaction of aluminum powder.

These SEM results and the explosion residues can be explained by the fact that the APP in MCM41@CS-APP decomposes in the high-temperature environment, which releases strong acids, such as polyphosphoric acid and pyrophosphoric acid.[38−40] These strong acids tend to dehydrate the surface of organic substances such as CS in the suppressant to form a colloidal carbon layer. Meanwhile, the gases including water vapor and NH_3 released from the thermal decomposition of APP and CS foam the carbon layer to form a porous colloidal carbon layer, which greatly hinders the direct contact between Al

https://doi.org/10.1021/acsomega.4c03871
ACS Omega 2024, 9, 44942−44955

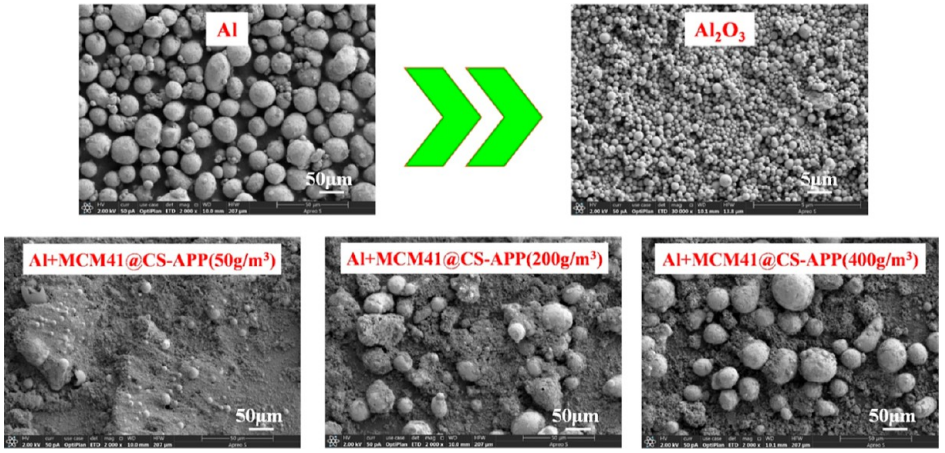

Figure 15. SEM images of the explosion residues of Al (19 μm) powder and Al/MCM41@CS-APP mixed dusts.

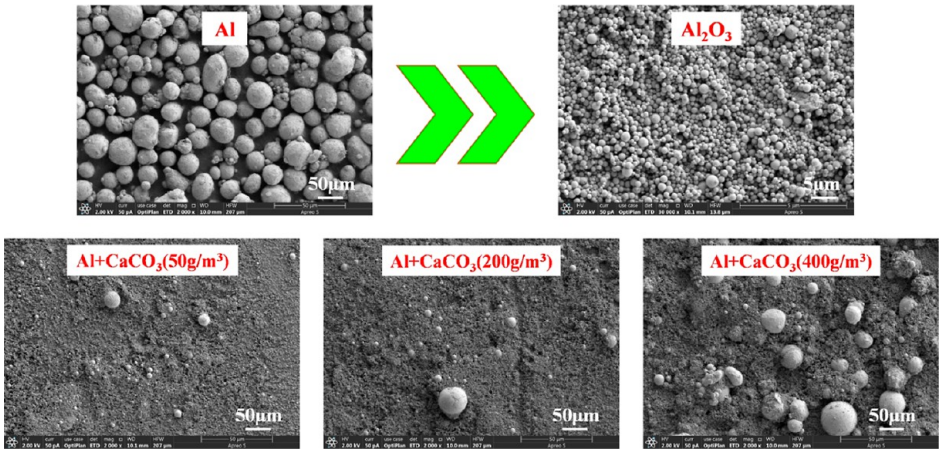

Figure 16. SEM images of the explosion residues of Al (19 μm) powder and Al/$CaCO_3$ mixed dusts.

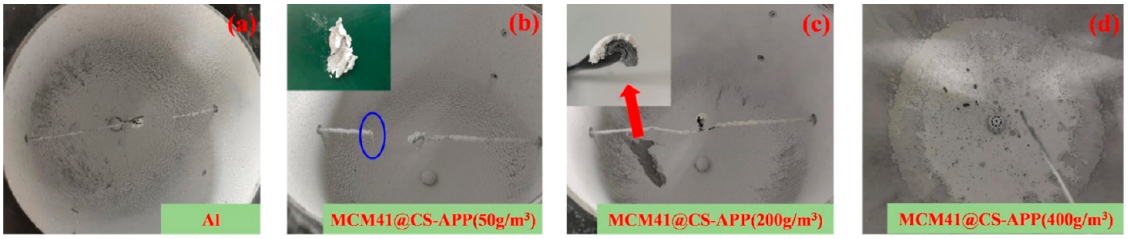

Figure 17. Images of the explosion residues of Al powder and Al/MCM41@CS-APP mixed dusts.

powder and oxygen, thereby suppressing the combustion and explosion of Al powder.

5.2. Thermogravimetric Analysis. In the above section, the suppression effects of MCM41@CS-APP and $CaCO_3$ were qualitatively analyzed by observing the morphologies of the mixed dust before and after explosion. In order to further understand their explosion suppression effects, TGA was conducted on Al powder (19 μm), MCM41@CS-APP, $CaCO_3$, and mixed dusts with $CaCO_3$/Al = 2:5, $CaCO_3$/Al = 4:5, MCM41@CS-APP/Al = 2:5, and MCM41@CS-APP/Al = 4:5, respectively, in a nitrogen atmosphere. Figure 18 shows the TG curves of Al powder, MCM41@CS-APP, and $CaCO_3$. The TG and derivative TG curves of the mixed dusts are shown in Figure 19.

From room temperature to 600 °C, trace moisture in aluminum powder is evaporated (Figure 18). As the temperature increased to over 600 °C, the weight of Al powder slightly rose due to the oxidation with air that produced amorphous alumina. The weight rapidly increases and then becomes constant as the temperature increases to over 800 °C. At this stage, the Al powder vigorously reacts to form Al_2O_3, but due to the incomplete reaction, the TG curve rises slowly from room temperature to 600 °C, mainly due to the evaporation of adsorbed water.[41] The TG curve declines dramatically as temperature increases to over 600 °C; $CaCO_3$ is decomposed in the high-temperature environment to form CaO and a large amount of CO_2.[42,43] The TG curve of MCM41@CS-APP is relatively complex. The adsorbed water in MCM41@CS-APP is evaporated as heated from room temperature to 320 °C. With the further increase of temperature, the APP in the suppressant is decomposed to release NH_3 and H_3PO_4. As the CS in the suppressant is heated, the dehydration of the sugar ring and the

https://doi.org/10.1021/acsomega.4c03871
ACS Omega 2024, 9, 44942−44955

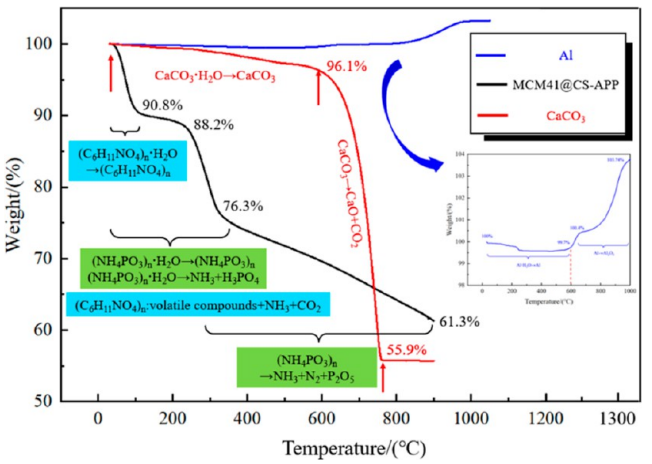

Figure 18. TG curves of Al powder (19 μm), MCM41@CS-APP, and $CaCO_3$.

degradation of the polymer unit generate a certain amount of NH_3. From 320 to 900 °C, the decomposition of APP continues to produce NH_3, as well as N_2, CO_2, and P_2O_5.[44,45]

As can be seen from Figure 19, the larger the proportion of the suppressant, the smaller the final mass percentage of mixed dust and the higher the initial oxidation temperature of Al powder. As shown in Figure 19a,b, when MCM41@CS-APP/Al = 2:5/4:5, the aluminum powder in the mixed dust started to oxidize at 835 and 850 °C, and the mass of Al/MCM41@CS-APP decreased by 9.8% and 15.7% at 900 °C, respectively. As Figure 19c shows, when $CaCO_3$/Al = 2:5, at 620−720 °C, the thermal decomposition of $CaCO_3$ made the mass of dust decrease by 10.1%; when the temperature reached 720 °C, the oxidation reaction of aluminum made the mass of dust begin to rise; and at 900 °C, the mass of Al/$CaCO_3$ decreased by 11.35%. As depicted in Figure 19d, when $CaCO_3$/Al = 4:5, the aluminum powder in Al/$CaCO_3$ began to oxidize and react at 740 °C, and the mass of Al/CaCO3 decreased by 19.6% at 900 °C.

5.3. X-ray Photoelectron Spectroscopy. In order to analyze the substances that may be present in the explosion products of the mixed dust, 200 g/m^3 of MCM41@CS-APP was added to the aluminum powder, and the full XPS spectra of Al and Al (500 g/m^3)/MCM41@CS-APP (200 g/m^3) were obtained after the explosion.

As shown in Figure 20a, after XPS analysis of the alumina produced by the explosion of aluminum powder, only three elements, namely, O, C, and Al, appeared in the full spectrum. In Figure 20b, after adding 200 g/m^3 of MCM41@CS-APP to the aluminum powder, three elements, P, Si, and N, appeared newly.

The XPS full spectrum of O 1s, C 1s, Al 2p, Si 2p, P 2p, and N 1s was obtained after peak splitting of the different elements in the product, as shown in Figure 21.

After the addition of MCM41@CS-APP, three peaks appeared in the O 1s spectra of the explosion products after the peak splitting process, corresponding to Al_2O_3, P−O bond, C−O bond, and O element in SiO_2 (Figure 21a). As shown in Figure 21b, three peaks appear in the C 1s spectra with C

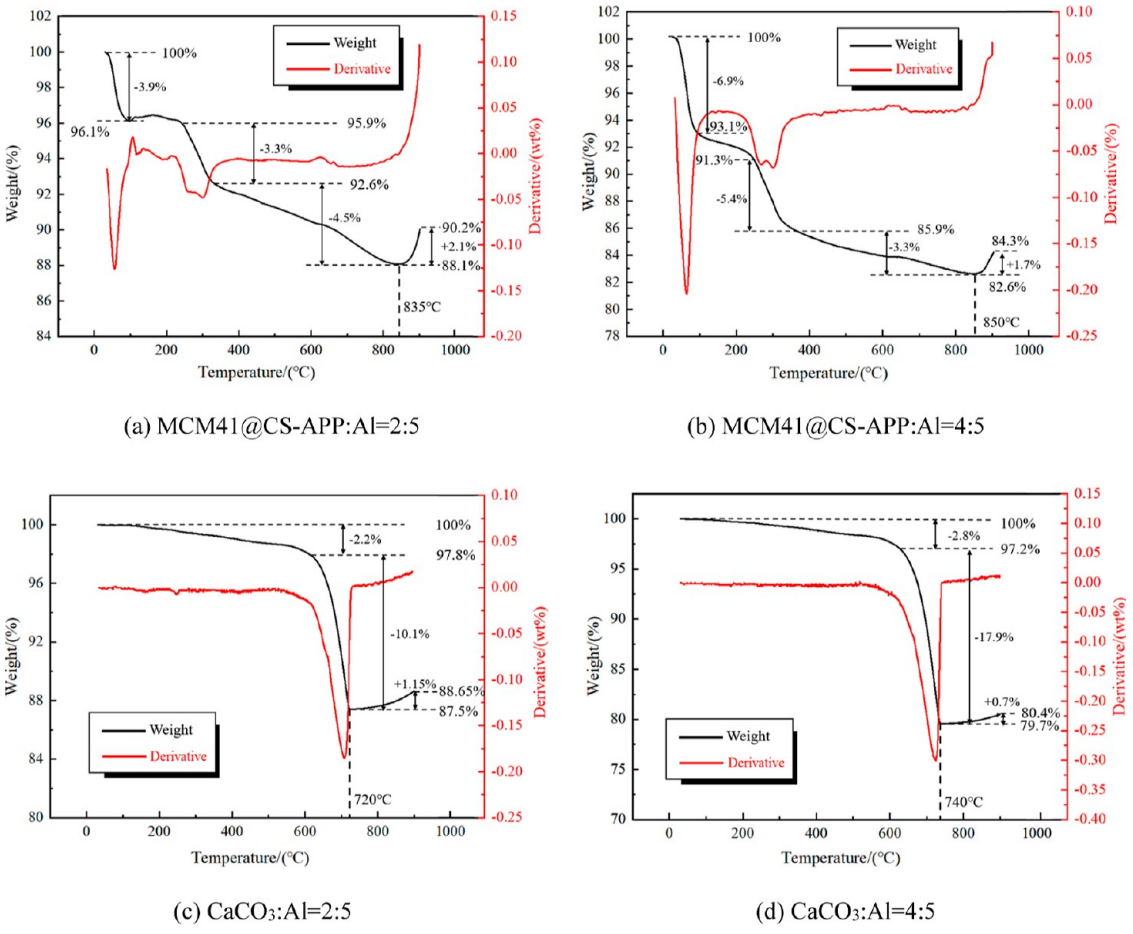

Figure 19. TG and derivative TG curves of Al/$CaCO_3$ and Al/MCM41@CS-APP with different ratios.

https://doi.org/10.1021/acsomega.4c03871
ACS Omega 2024, 9, 44942−44955

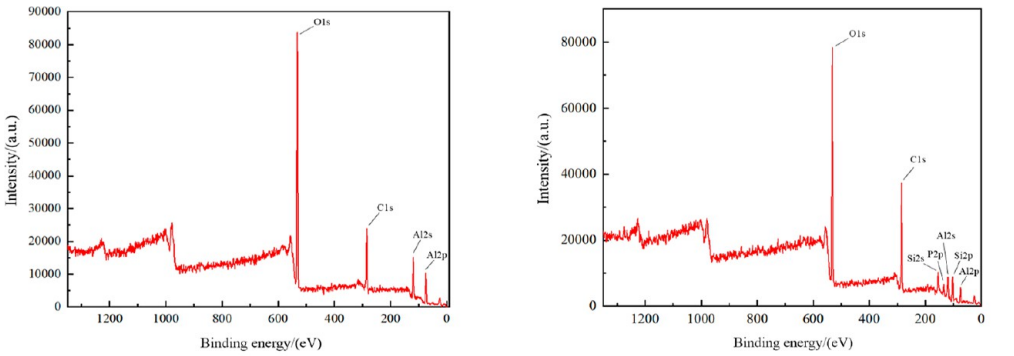

(a) XPS full spectrum of Al (b) XPS full spectrum of Al/MCM41@CS-APP(200 g/m^3)

Figure 20. XPS full spectrum.

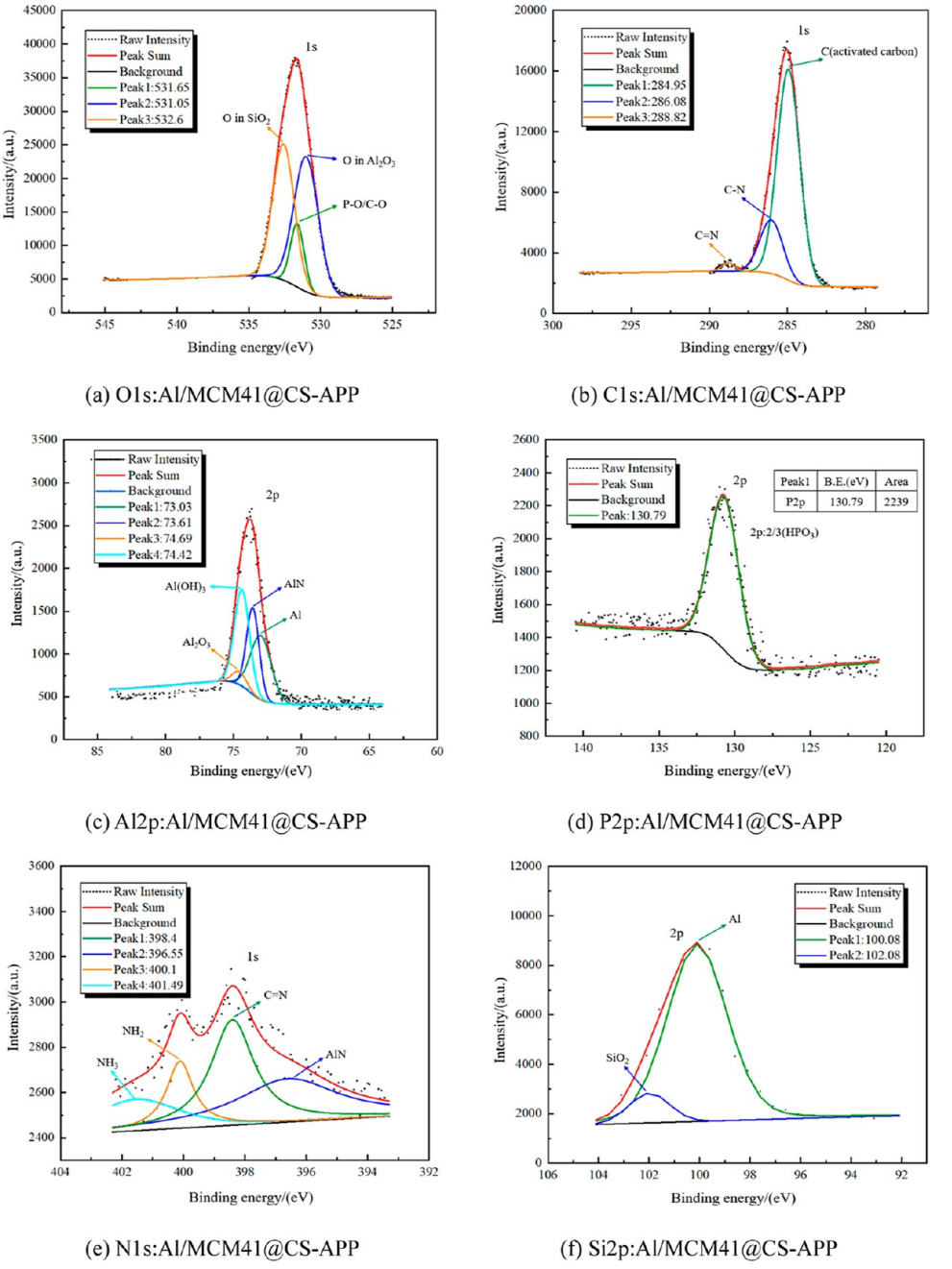

(a) O1s:Al/MCM41@CS-APP (b) C1s:Al/MCM41@CS-APP

(c) Al2p:Al/MCM41@CS-APP (d) P2p:Al/MCM41@CS-APP

(e) N1s:Al/MCM41@CS-APP (f) Si2p:Al/MCM41@CS-APP

Figure 21. XPS full spectrum of O 1s, C 1s, Al 2p, P 2p, N 1s, and Si 2p in Al/MCM41@CS-APP explosion products.

https://doi.org/10.1021/acsomega.4c03871
ACS Omega 2024, 9, 44942−44955

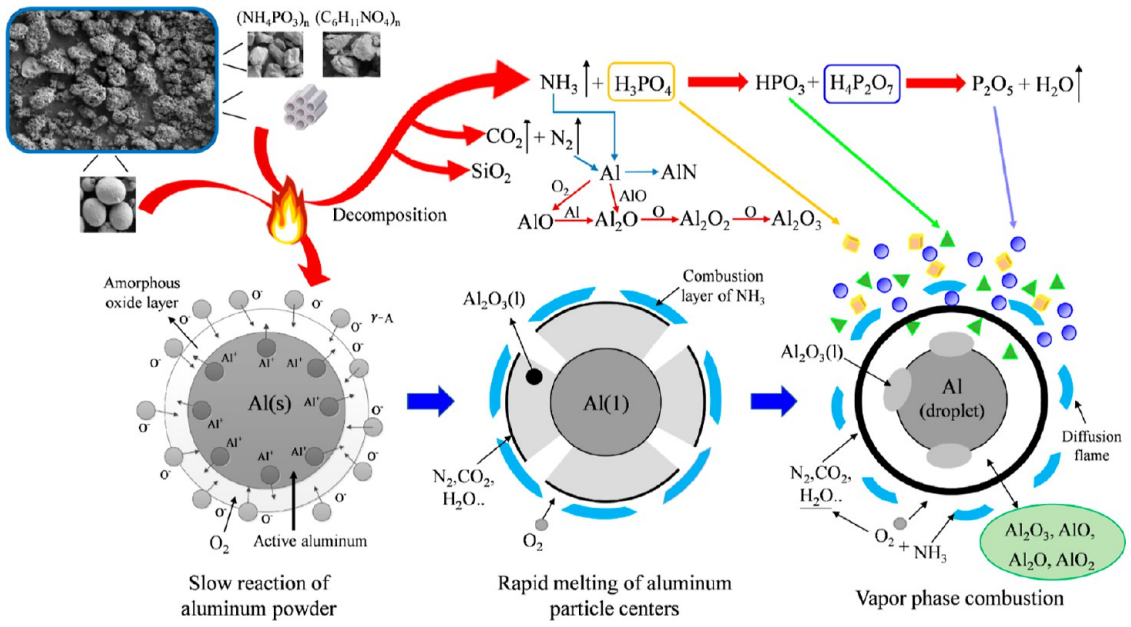

Figure 22. Schematic diagram of the mechanism of inhibition of aluminum particle explosion by MCM41@CS-APP.

elements originating from activated carbon, the C−N bond, and the C═N bond.[46] As illustrated in Figure 21c, four peaks in the Al 2p spectra of the explosion products were obtained after the peak splitting process, and after analysis, it was concluded that the four peaks corresponded to Al, AlN, $Al(OH)_3$, and Al_2O_3, respectively. Under the inhibition effect of MCM41@CS-APP, most of the explosion products of Al/MCM41@CS-APP consisted of alumina particles and some unreacted aluminum particles. $Al(OH)_3$ may also be present. After the addition of MCM41@CS-APP at a concentration of 200 g/m^3, the P element was considered to belong to phosphoric acid and other compounds such as P_2O_5, and the N element was derived from AlN, NH_2, NH_3, and C═N bonding.[47] In addition, the selected molecular sieve (MCM-41) specification is all-silicon, which combines Si with O to form SiO_2 in high-temperature environments.[48]

6. RESULTS AND DISCUSSION

Through the XPS analysis of Al/MCM41@CS-APP explosion products, combined with SEM analysis and TGA, it was obtained that the inhibitory effect of MCM41@CS-APP on the explosion of aluminum powder was reflected in the condensation phase and gas phase. From the condensed-phase aspect, the APP loaded by MCM-41 is thermally decomposed to phosphoric acid and phosphates with CS as the carbon source, expanding and carbonizing to form a dense carbon layer under the action of acid and gas sources.[49−52] The charcoal layer can effectively prevent the penetration of oxygen and the diffusion of the combustible gas, which inhibits the oxidation and combustion of Al powder to great extents. From the gas-phase aspect, the amino group in CS is converted into NH_3 at the high temperatures, and the reaction of APP produces large amounts of inert gases, such as NH_3, CO_2, and N_2. These gas products dilute O_2 and take the heat produced from the combustion away. The free radicals, PO$^\bullet$ and HPO$^\bullet$, generated from APP at the high temperatures can capture the active free radicals, such as H$^\bullet$, HO$^\bullet$, O$^\bullet$, and so on, as shown below, which makes it very difficult to continue the combustion chain reaction.[53−55]

$$H_3PO_4 \rightarrow HPO_2 + PO^\bullet + HPO^\bullet$$

$$H^\bullet + PO^\bullet \rightarrow HPO^\bullet$$

$$H^\bullet + HPO^\bullet \rightarrow H^\bullet + PO^\bullet$$

$$HO^\bullet + PO^\bullet \rightarrow HPO^\bullet + O^\bullet$$

According to the above analysis, the suppression mechanism of aluminum powder explosion by MCM41@CS-APP is obtained, as shown in Figure 22.

7. CONCLUSIONS

In this paper, the inhibition effect of MCM41@CS-APP and $CaCO_3$ on the explosion flame and explosion pressure of aluminum powder (500 g/m^3) was investigated; the inhibition performance of MCM41@CS-APP and $CaCO_3$ on the explosion of aluminum powder was compared in various aspects such as flame development, pressure changes, and initial material analysis; and the inhibition mechanisms of MCM41@CS-APP on the explosion of aluminum powder were obtained through SEM, TG, and XPS analyses, and the following conclusions were obtained:

(1) The P_{max} of the mixed dust decreased continuously with the increase of the deflagration suppressant concentration, and the decreasing trend of Al/MCM41@CS-APP was more significant. When the concentrations of MCM41@CS-APP and $CaCO_3$ reached 400 g/m^3, the P_{max} of mixed dust (Al = 19 μm) was 0.133 and 0.364 MPa, which decreased by 81.3% and 48.9%, respectively; the P_{max} of mixed dust (Al = 30 μm) was not significant.

(2) The particle size of aluminum powder has an impact on the explosion effect. Aluminum powder with a smaller particle size burns more strongly and has a longer combustion process. Adding the same concentration of the deflagration suppressant, Al/MCM41@CS-APP produced a significantly weaker flame optimum than that of Al/$CaCO_3$, and the burning time of Al/MCM41@CS-APP was shorter.

https://doi.org/10.1021/acsomega.4c03871
ACS Omega 2024, 9, 44942−44955

(3) The larger the proportion of the suppressant, the smaller the final mass percentage of mixed dust and the higher the initial oxidation temperature of Al powder; when $CaCO_3$/Al = 2:5, MCM41@CS-APP/Al = 2:5, $CaCO_3$/Al = 4:5, and MCM41@CS-APP/Al = 4:5, the initial oxidation reaction temperatures of aluminum are 720, 835, 740, and 850 °C, respectively.

(4) Under the high-temperature environment, APP and CS in MCM41@CS-APP react synergistically to generate a gelatinous carbon layer; APP and CS molecules also release a large number of inert gases; and the free radicals generated by APP, such as $PO^{\bullet}$ and $HPO^{\bullet}$, are able to capture reactive free radicals. The inhibition of the explosion of aluminum powders by MCM41@CS-APP has been described in the condensation phase and the gas phase.

As a self-developed solid powder suppressant, the preliminary results show that it has a good suppressant effect (compared with the conventional solid suppressant calcium carbonate). In order to explore whether MCM41@CS-APP has application value, it will be considered in the future to compare its explosion suppression performance with $NH_4H_2PO_4$ or MCA materials under different initial conditions.

AUTHOR INFORMATION

Corresponding Author

Haiyan Chen − *College of Safety and Environmental Engineering, Shandong University of Science and Technology, Qingdao 266590, P. R. China; Mine Disaster Prevention and Control-Ministry of State Key Laboratory Breeding Base, Shandong University of Science and Technology, Qingdao 266590, P. R. China;* orcid.org/0000-0001-7500-1962; Phone: + 86-13853233472; Email: sdustchy@sdust.edu.cn

Authors

Xinyu Li − *College of Safety and Environmental Engineering, Shandong University of Science and Technology, Qingdao 266590, P. R. China*

Yansong Zhang − *College of Safety and Environmental Engineering, Shandong University of Science and Technology, Qingdao 266590, P. R. China*

Chunmiao Yuan − *Fire & Explosion Protection Laboratory, Northeastern University, Shenyang 110004, P. R. China*

Hongzhao Wei − *College of Safety and Environmental Engineering, Shandong University of Science and Technology, Qingdao 266590, P. R. China*

Wenxue Sun − *College of Safety and Environmental Engineering, Shandong University of Science and Technology, Qingdao 266590, P. R. China*

Zhangjie Lu − *College of Safety and Environmental Engineering, Shandong University of Science and Technology, Qingdao 266590, P. R. China*

Qingzhou Zhang − *College of Safety and Environmental Engineering, Shandong University of Science and Technology, Qingdao 266590, P. R. China*

Complete contact information is available at: https://pubs.acs.org/10.1021/acsomega.4c03871

Notes

The authors declare no competing financial interest.

ACKNOWLEDGMENTS

This work was supported by the Key Project of the Natural Science Foundation of Shandong Province (project no. ZR2022ME183) and the National Natural Science Foundation of China (project no. 52374215).

REFERENCES

(1) Dufaud, O.; Traoré, M.; Perrin, L.; Chazelet, S.; Thomas, D. Experimental investigation and modelling of aluminum dusts explosions in the 20 L sphere. *J. Loss Prev. Process. Ind.* **2010**, *23* (2), 226−236.

(2) Beckstead, M. W.; Liang, Y.; Pudduppakkam, K. V. Numerical Simulation of Single Aluminum Particle Combustion (Review). *Combust. Explos. Shock Waves* **2005**, *41* (6), 622−638.

(3) Vignes, A.; Krietsch, A.; Dufaud, O.; Santandréa, A.; Perrin, L.; Bouillard, J. Course of explosion behaviour of metallic powders-From micron to nanosize. *J. Hazard. Mater.* **2019**, *379*, 120767.

(4) Wang, Q.; Fang, X.; Shu, C.; Wang, Q.; Sheng, Y.; Jiang, J.; Sun, Y.; Sheng, Z. Minimum ignition temperatures and explosion characteristics of micron-sized aluminium powder. *J. Loss Prev. Process. Ind.* **2020**, *64*, 104076.

(5) Dastidar, A.; Amyotte, P. Determination of Minimum Inerting Concentrations for Combustible Dusts in a Laboratory-Scale Chamber. *Process Saf. Environ. Prot.* **2002**, *80* (6), 287−297.

(6) Jérôme, T.; Vingerhoets, J.; et al. Suppression of metal dust deflagrations. *J. Loss Prev. Process. Ind.* **2015**, *36*, 244−251.

(7) Mintz, K. J.; Bray, M. J.; Zuliani, D. J.; Amyotte, P.; Pegg, M. Inerting of fine metallic powders. *J. Loss Prev. Process. Ind.* **1996**, *9* (1), 77−80.

(8) Amrogowicz, J.; Kordylewski, W. Effectiveness of dust explosion suppression by carbonates and phosphates. *Combust. Flame* **1991**, *85* (3−4), 520−522.

(9) Jiang, H.; Bi, M.; Gao, W. Flame inhibition of aluminum dust explosion by $NaHCO_3$ and $NH_4H_2PO_4$. *Combust. Flame* **2019**, *200*, 97−114.

(10) Zhang, S.; Bi, M.; Jiang, H.; Gao, W. Suppression effect of inert gases on aluminum dust explosion. *Powder Technol.* **2021**, *388*, 90−99.

(11) Zhang, T.; Jiang, H.; Shang, S.; Zhang, K.; Gao, W. Synthesis of aluminum hydroxide/Zinc borate composite inhibitor and its inhibition effect on aluminum dust explosion. *Chem. Eng. Sci.* **2022**, *248* (Part B), 117204.

(12) Zhang, T.; Jiang, H.; Zhang, K.; Zhu, C.; Xue, C.; Zhang, Z.; Xu, J.; Gao, W. Inhibition effect of aluminum dust explosions by one novel zinc borate. *Chem. Eng. Sci.* **2022**, *255*, 117682.

(13) Dai, L. L.; Hao, L.; Kang, W.; Xu, W.; Shi, N.; Wei, H. Inhibition of different types of inert dust on aluminum powder explosion. *Chin. J. Chem. Eng.* **2020**, *28* (7), 1941−1949.

(14) Ke, Y.; Meng, X. B.; Pan, Z. C.; Wang, Z.; Zhang, Y. S. Effect and mechanism of KH_2PO_4/SiO_2 composite powder in inhibiting aluminum dust deflagration. *Explos. Shock Waves* **2021**, *42* (6), 062101-1.

(15) Deng, J.; Jiao, Q. U.; Qiu-hong, W.; Yu-feng, Y. Inhibition of ABC/MCA powder on explosion characteristics of aluminum metal powder. *J. Xi'an Univ. Eng. Sci. Technol.* **2020**, *40* (1), 18−23.

(16) Jiang, S. D.; Bai, Z. M.; Tang, G.; Song, L.; Stec, A. A.; Hull, T. R.; Hu, Y.; Hu, W. Z. Synthesis of mesoporous silica@Co-Al layered double hydroxide spheres: layer-by-layer method and their effects on the flame retardancy of epoxy resins. *ACS Appl. Mater. Interfaces* **2014**, *6* (16), 14076−14086.

(17) Qian, Y.; Wei, P.; Jiang, P.; Li, Z.; Yan, Y.; Ji, K. Aluminated mesoporous silica as novel high-effective flame retardant in polylactide. *Compos. Sci. Technol.* **2013**, *82*, 1−7.

(18) Zhu, H.; Liang, C.; Yan, W.; Overbury, S. H.; Dai, S. Preparation of highly active silica-supported Au catalysts for CO oxidation by a solution-based technique. *J. Phys. Chem. B* **2006**, *110* (22), 10842−10848.

(19) Rafia, R.; Gul, A. R.; Lee, I. G.; Baek, S. H.; Kailasa, S. K.; Iqbal, N.; Cho, E. J.; Lee, M.; Park, T. J. Photo-induced reactions for

disassembling of coloaded photosensitizer and drug molecules from upconversion-mesoporous silica nanoparticles: An effective synergistic cancer therapy. *Mater. Sci. Eng., C* **2020**, *110*, 110545.
(20) Li, C.; Zhang, G.; Yuan, B. Exceptional performance of flame-retardant polyurethane foam: the suppression effect on explosion pressure and flame propagation of methane-air premixed gas. *J. Mater.* **2023**, *16* (24), 7602.
(21) Prabhakar, M. N.; Raghavendra, G. M.; Vijaykumar, B. V. D.; Patil, K.; Seo, J.; Jung-il, S. Synthesis of a novel compound based on chitosan and ammonium polyphosphate for flame retardancy applications. *Cellulose* **2019**, *26*, 8801−8812.
(22) Malucelli, G. Flame-Retardant Systems Based on Chitosan and Its Derivatives: State of the Art and Perspectives. *Molecules* **2020**, *25* (18), 4046.
(23) Chen, C.; Gu, X.; Jin, X.; Sun, J.; Zhang, S. The effect of chitosan on the flammability and thermal stability of polylactic acid/ammonium polyphosphate biocomposites. *Carbohydr. Polym.* **2017**, *157*, 1586−1593.
(24) Hu, S.; Song, L.; Pan, H.; Hu, Y. Thermal properties and combustion behaviors of chitosan based flame retardant combining phosphorus and nickel. *Ind. Eng. Chem. Res.* **2012**, *51* (9), 3663−3669.
(25) Khan, D.; Shaily. Synthesis and catalytic applications of organo-functionalized MCM-41 catalyst: A review. *Appl. Organomet. Chem.* **2023**, *37* (3), No. e7007.
(26) Lv, P.; Liu, Z.; Zhao, J.; Pang, L. Inerting effect of $CaCO_3$ powder on flame spread of wood dust layer. *J. Loss Prev. Process. Ind.* **2023**, *82*, 105000.
(27) Yuan, G.; Kuai, N.; Liu, L.; Huang, W. Experiment investigation on the inhibition effectiveness of $CaCO_3$ on dust explosions. *Fire Sci. Technol.* **2014**, *33* (2), 128−130.
(28) Wu, Y.; Yuan, J.; Kuai, N.; Huang, W. Experimental study on the effect of carbonate on dust explosion pressure in confined space. *China Saf. Sci. J.* **2010**, *20*, 92−96.
(29) Chen, Z.; Jiang, J.; Yu, Y.; Zhang, Q.; Chen, T.; Ni, L. Layer-by-layer assembled diatomite based on chitosan and ammonium polyphosphate to increase the fire safety of unsaturated polyester resins. *Powder Technol.* **2020**, *364*, 36−48.
(30) Li, G.; Yang, H.; Yuan, C.; Eckhoff, R. K. A catastrophic aluminium-alloy dust explosion in China. *J. Loss Prev. Process. Ind.* **2016**, *39*, 121−130.
(31) International Organization for Standardization. *Explosion Protection Systems Part 1: Determination of Explosion Indices of Combustible Dusts in Air*, 1985. ISO 6184-1.
(32) Standardization Administration of the People's Republic of China. *Determination for Minimum Explosive Concentration of Dust Clouds*, 2018. GB/T 16425-2018.
(33) Zhang, J.; Ren, X.; Jia, H.; Cui, Z.; Xiong, N.; Xiao, B.; Han, X. Effect of particle size distribution on explosion intensity of aluminum powder. *Process Saf. Prog.* **2023**, *42* (1), 186−193.
(34) Kim, W.; Saeki, R.; Ueno, Y.; Johzaki, T.; Endo, T.; Choi, K. Effect of particle size on the minimum ignition energy of aluminum powders. *Powder Technol.* **2023**, *415*, 118190.
(35) Jiang, P. Z.; Fan Tang, G.; Wang, Y. C.; Han, Y. Explosive property and combustion kinetics of grain dust with different particle sizes. *Heliyon* **2020**, *6*, No. e03457.
(36) Dastidar, A. G.; Amyotte, P. R.; Going, J.; Chatrathi, K. Flammability limits of dusts: minimum inerting concentrations. *Process Saf. Prog.* **1999**, *18* (1), 56−63.
(37) Yang, D.; Zhou, M.; Ye, D.; et al. A Flexible and Breathable Ammonium Polyphosphate/Chitosan/Mwcnt Doped Pedot: Pss Coating Decorated Carbon Cloth for High-Efficiency Flame Retardancy and Electromagnetic Interference Shielding Applications. *Surface. Interfac.* **2024**, *51*, 104786.
(38) Gu, J.; Zhang, G.; Dong, S.; Zhang, Q. y.; Kong, J. Study on preparation and fire-retardant mechanism analysis of intumescent flame-retardant coatings. *Surf. Coat. Technol.* **2007**, *201* (18), 7835−7841.
(39) Zhang, T.; Zhang, Z.; Zhu, C.; Gao, W. Inhibition effects of aluminum dust explosions by various kinds of ammonium polyphosphate. *J. Loss Prev. Process. Ind.* **2023**, *83*, 105083.
(40) Alongi, J.; Carosio, F.; Malucelli, G. Layer by layer complex architectures based on ammonium polyphosphate, chitosan and silica on polyester-cotton blends: flammability and combustion behaviour. *Cellulose* **2012**, *19*, 1041−1050.
(41) Johnson, C. E.; Fallis, S.; Chafin, A. P.; Groshens, T. J.; Higa, K. T.; Ismail, I. M. K.; Hawkins, T. W. Characterization of Nanometer- to Micron-Sized Aluminum Powders: Size Distribution from Thermogravimetric Analysis. *J. Propul. Power* **2007**, *23* (4), 669−682.
(42) Galan, I.; Glasser, F. P.; Andrade, C. Calcium carbonate decomposition. *J. Therm. Anal. Calorim.* **2013**, *111*, 1197−1202.
(43) Li, Y.-N.; Jiao, F.; Wen, L. Research on the Effects of $CaCO_3$ on Minimum Ignition Energy of Metal Dust. *J. North Univ. China* **2014**, *35* (05), 594−598.
(44) Amyotte, P. R. Solid inertants and their use in dust explosion prevention and mitigation. *J. Loss Prev. Process. Ind.* **2006**, *19*, 161−173.
(45) Huang, C.; Yuan, B.; Zhang, H.; Zhao, Q.; Li, P.; Chen, X.; Yun, Y.; Chen, G.; Feng, M.; Li, Y. Investigation on thermokinetic suppression of ammonium polyphosphate on sucrose dust deflagration: Based on flame propagation, thermal decomposition and residue analysis. *J. Hazard. Mater.* **2021**, *403*, 123653.
(46) Castrovinci, A.; Camino, G.; Drevelle, C.; Duquesne, S.; Magniez, C.; Vouters, M. Ammonium polyphosphate−aluminum trihydroxide antagonism in fire retarded butadiene−styrene block copolymer. *Eur. Polym. J.* **2005**, *41* (9), 2023−2033.
(47) Dante, R. C.; Sanchez-Arevalo, F. M.; Chamorro-Posada, P.; Vazquez-Cabo, J.; Huerta, L.; Lartundo-Rojas, L.; Santoyo-Salazar, J.; Solorza-Feria, O. Supramolecular intermediates in the synthesis of polymeric carbon nitride from melamine cyanurate. *J. Solid State Chem.* **2015**, *226*, 170−178.
(48) Candela-Noguera, V.; Alfonso, M.; Amorós, P.; et al. In-depth study of factors affecting the formation of MCM-41-type mesoporous silica nanoparticles[J]. *Microporous Mesoporous Mater.* **2024**, *363*, 112840.
(49) Chen, X. X.; Fang, F.; Du, T.; et al. Preparation and properties of chitosan-potassium alginate flame retardant coating via layer-by-layer self-assembly technology. *Polym. Mater. Sci. Eng.* **2016**, *32* (7), 121−124.
(50) Xiao, Y.; Zheng, Y.; Wang, X.; Chen, Z.; Xu, Z. Preparation of a chitosan-based flame-retardant synergist and its application in flame-retardant polypropylene. *J. Appl. Polym. Sci.* **2014**, *131* (19), 40845.
(51) Jie, B.; Baoxia, X.; Yang, Y.; et al. Flame Retardancy and Smoke Suppression of Intumescent Flame Retardant PP With Chitosan/Ammonium Phosphate. *Eng. Plast. Appl.* **2017**, *45* (7), 119−123.
(52) Fang, F.; Zhang, X.; Meng, Y.; Gu, Z.; Bao, C.; Ding, X.; Li, S.; Chen, X.; Tian, X. Intumescent flame retardant coatings on cotton fabric of chitosan and ammonium polyphosphate via layer-by-layer assembly. *Surf. Coat. Technol.* **2015**, *262*, 9−14.
(53) Wang, G.; Yang, J. Thermal degradation study of fire resistive coating containing melamine polyphosphate and dipentaerythritol. *Prog. Org. Coat.* **2011**, *72* (4), 605−611.
(54) Zhang, L. L.; Liu, A. H. Synergistic Effect and Application of Phosphorus/Silicon Flame Retardant. *China Plast. Ind.* **2008**, *29*, 203−204.
(55) Lu, H.; Ma, X.; Hongxia, Y. Recent progress in phosphorus flame retardants. *N. Chem. Mater.* **2001**, *29* (12), 7−10.

https://doi.org/10.1021/acsomega.4c03871
ACS Omega 2024, 9, 44942−44955